Supplementary material for

Multiscale Aspects of an Extreme Precipitation Event over Nepal in September 2024

Hatsuki Fujinami[1*], Nobuhiro Takahashi[1], Hironari Kanamori[2], Yota Sato[3], Sojiro Sunako[4], Masaya Kato[1], Atsushi Higuchi[5,6,7], Indira Kadel[8], Dibas Shrestha[9], Rijan B Kayastha[10] and Koji Fujita[11]

1 Institute for Space-Earth Environmental Research, Nagoya University, Furo-cho, Chikusa-ku, Nagoya 464-8601, Japan

2 Faculty of Business Administration, Kobe Gakuin University, 1-1-3 Minatojima, Chuo-ku, Kobe 650-8586, Japan

3 Institute of Science and Technology Austria, Am Campus 1, 3400 Klosterneuburg, Austria

4 Snow and Ice Research Center, National Research Institute for Earth Science and Disaster Resilience, 187-16 Maeyama, Suyoshi-cho, Nagaoka 940-0821, Japan

5 Center for Environmental Remote Sensing, Chiba University, 1-33 Yayoi-cho, Inage-ku, Chiba 263-8522, Japan

6 Research Institute of Disaster Medicine, Chiba University, 1-8-1 Inohana, Chuo-ku, Chiba 260-0856, Japan

7 Typhoon Science and Technology Research Center, Yokohama National University, 79-5 Tokiwadai, Hodogaya-ku, Yokohama 240-8501, Japan

8 Department of Hydrology and Meteorology, Babarmahal, Kathmandu, Nepal

9 Central Department of Hydrology and Meteorology, Tribhuvan University, Kirtipur, Kathmandu, Nepal

10 Department of Environmental Science, School of Science, Kathmandu University, Dhulikhel, Nepal

11 Graduate School of Environmental Studies, Nagoya University, Furo-cho, Chikusa-ku, Nagoya 464-8601, Japan

*Corresponding author. Email: hatsuki@nagoya-u.jp

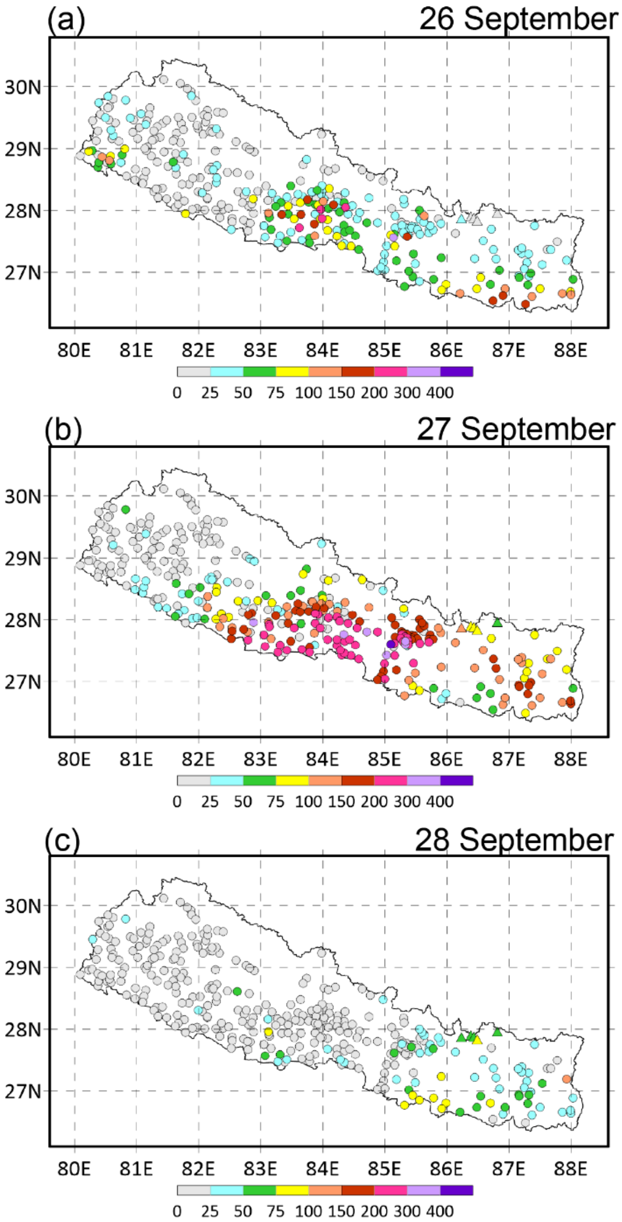

Fig. S1 (a) Daily precipitation (mm d^{-1}) on (a) 26 September, (b) 27 September, and (c) 28 September 2024. Circles indicate the locations of the rain gauges of the Department of Hydrology and Meteorology (DHM) in Nepal, while the triangles indicate the locations of the rain gauges in the Rolwaling and Khumbu regions

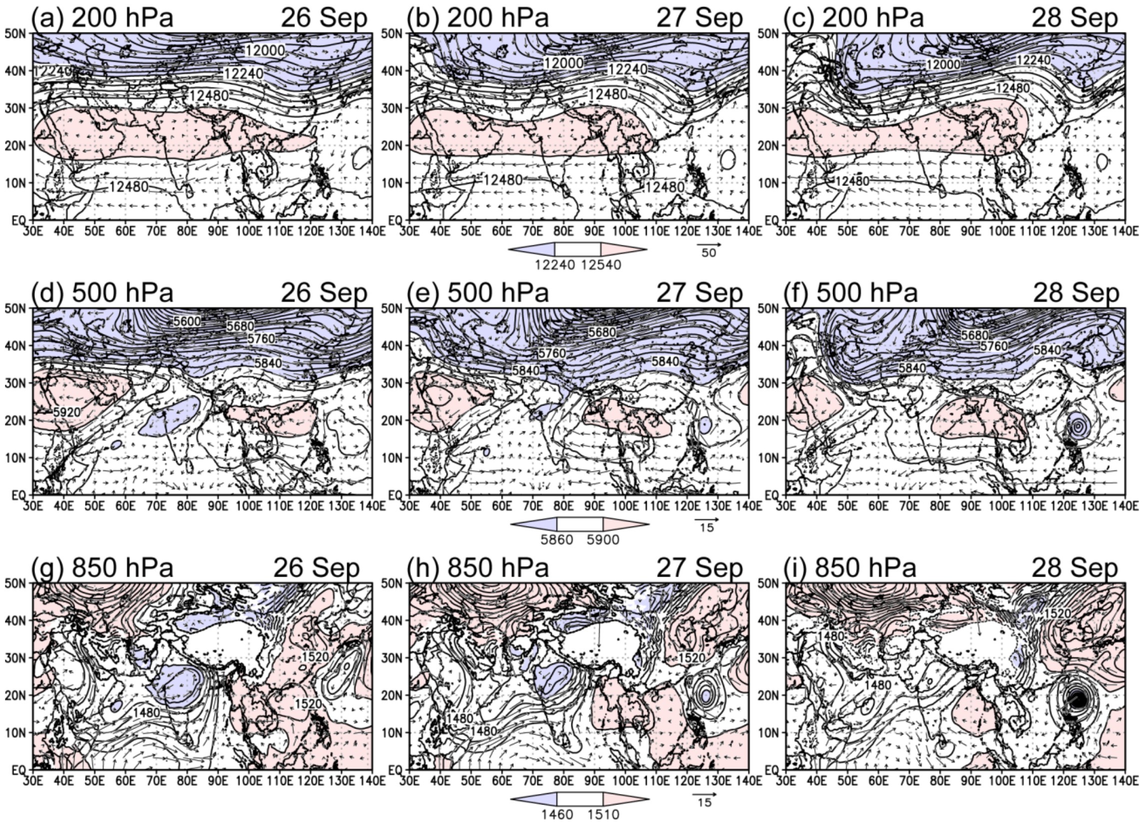

Fig. S2 Spatial distribution of geopotential height (contours and shading; gpm) and wind field (vectors; m s^{-1}) at 200 hPa on (a) 26 September, (b) 27 September, and (c) 28 September 2024. Contour interval for geopotential height is 60 gpm. (d)–(f) As in (a)–(c), respectively, but for 500 hPa. Contour interval for geopotential height is 20 gpm. (g)–(i) As in (a)–(c), respectively, but for 850 hPa. Contour interval for geopotential height is 10 gpm

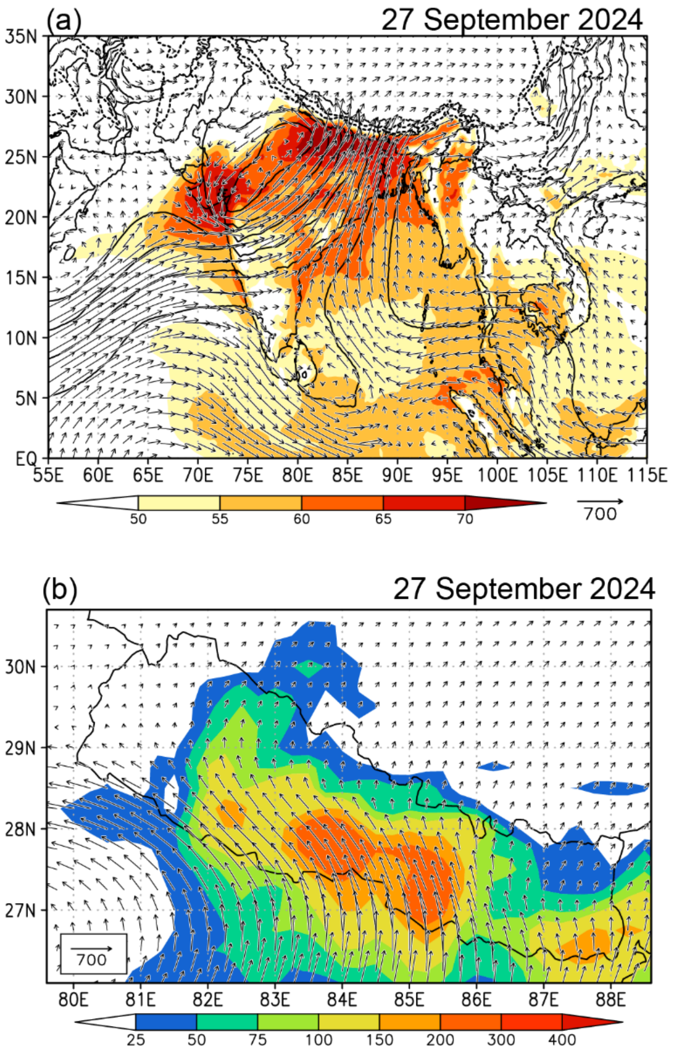

Fig. S3 (a) Spatial distribution of total column water vapor (shading; mm), vertically integrated water vapor flux (WVF) (vectors; kg m^{-1} s^{-1}), and 850-hPa geopotential height (gpm) on 27 September. Contour interval for geopotential height is 10 gpm. (b) Distribution of WVF convergence (shading; mm d^{-1}) and vertically integrated WVF (vectors; kg m^{-1} s^{-1}) on 27 September 2024

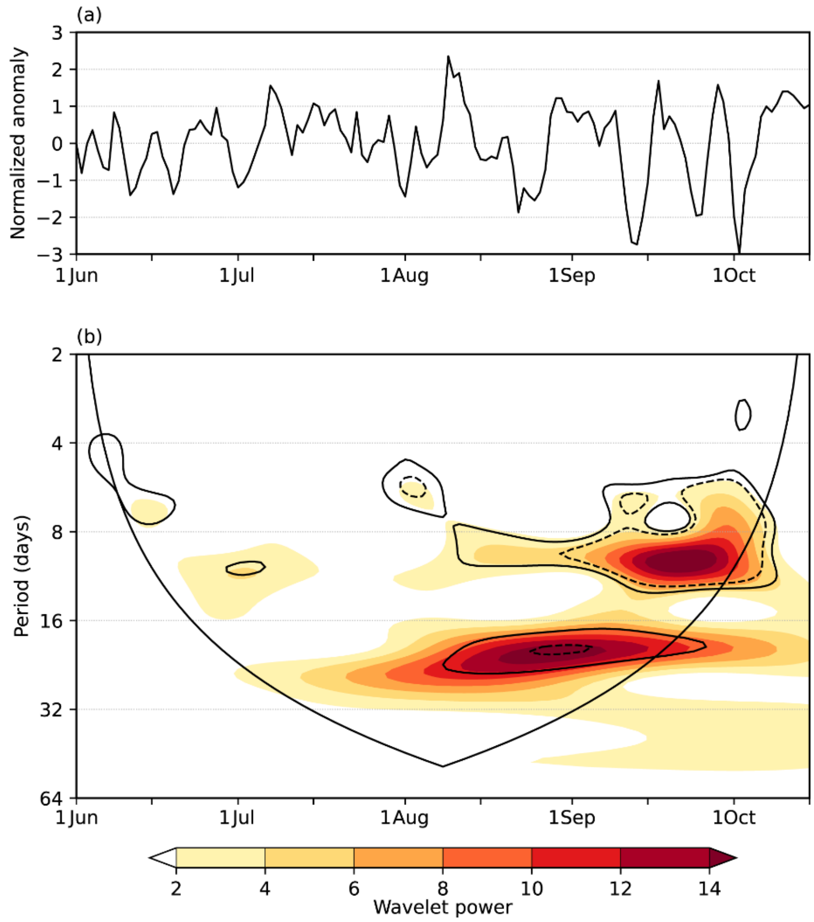

Fig. S4 (a) Time series of normalized outgoing longwave radiation (OLR) anomalies averaged over 15°–23° N, 85°–95° E (Bay of Bengal region) for the period of 1 June to 15 October 2024 and (b) its wavelet power spectrum (shading). The wavelet analysis was performed using the Morlet wavelet. The thick black and dashed contours indicate the 95% and 99% confidence levels against a red-noise spectrum, respectively. The black curve denotes the cone of influence.

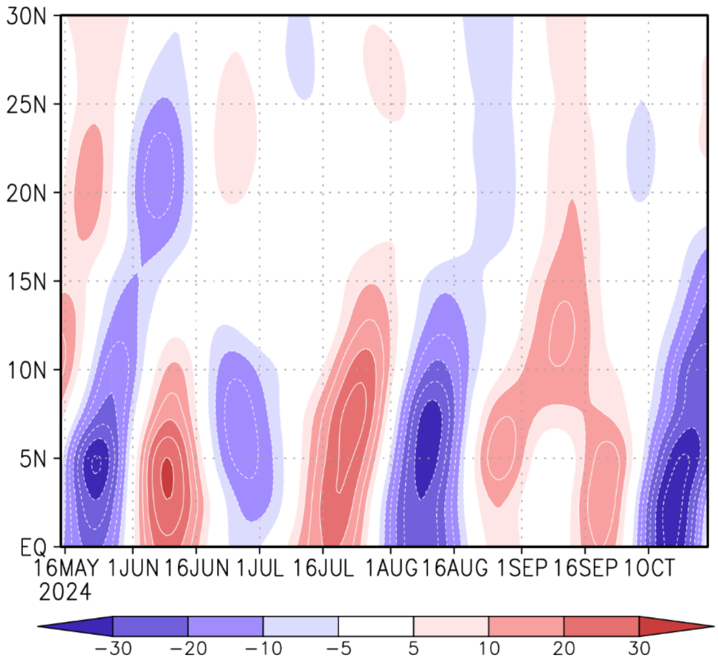

Fig. S5 Latitude–time section of 25–90-day filtered outgoing longwave radiation (OLR) anomalies (W m^{-2}) averaged over 85°–90° E. Daily anomalies of OLR were computed by subtracting the first three harmonics of the annual cycle (approximately 120 days); 25–90-day anomalies were obtained by applying a Lanczos bandpass filter to the detrended daily anomalies (Kukuchi 2021)

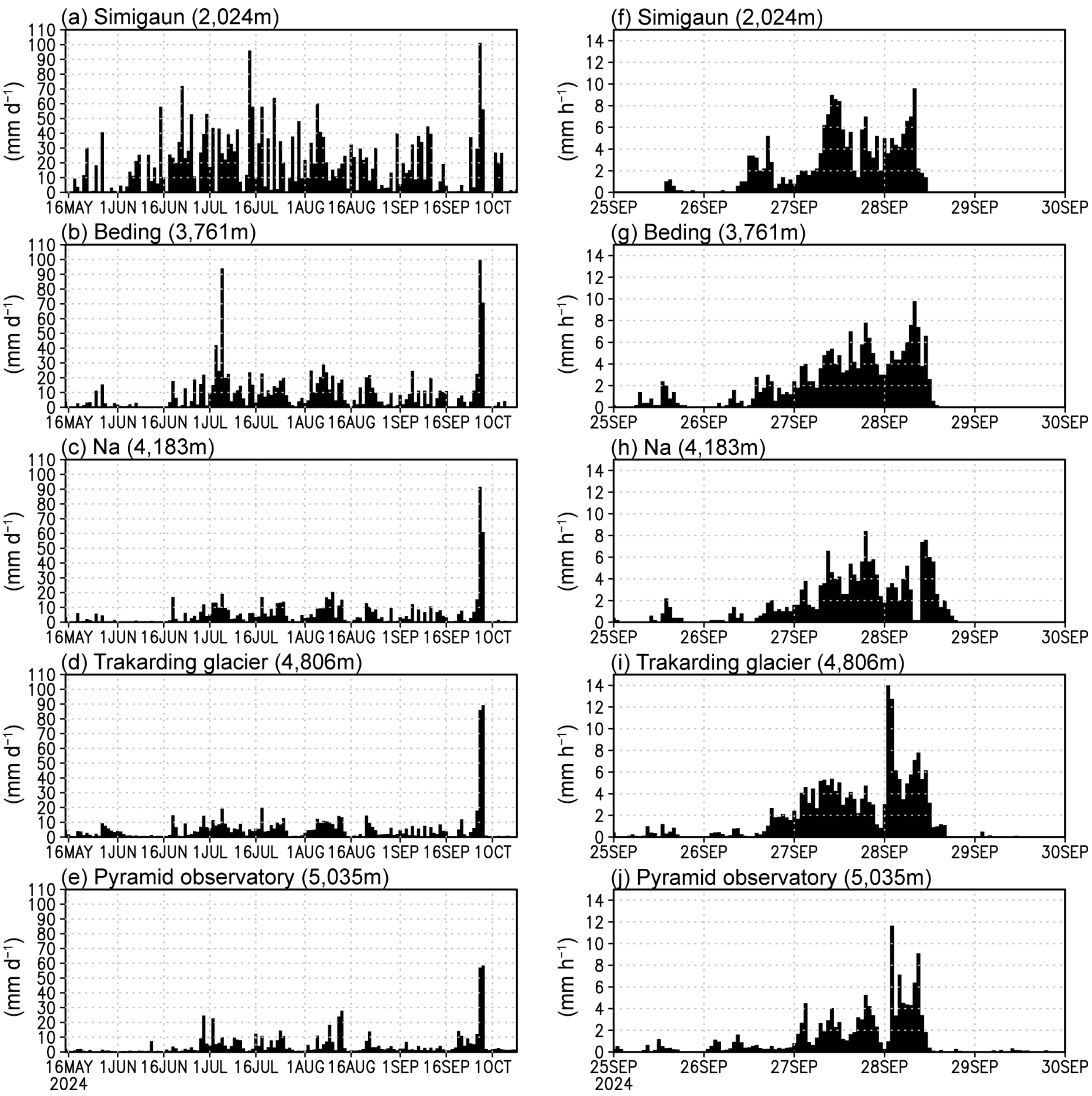

Fig. S6 Time series of daily precipitation (mm d^{-1}) at (a) Simigaun, (b) Beding, (c) Na, and (d) Trambau Glacier stations and (e) Pyramid observatory. (f)–(j) As in (a)–(e), respectively, but for hourly precipitation (mm h^{-1}) from 00:00 UTC on 25 September to 00:00 UTC on 30 September 2024

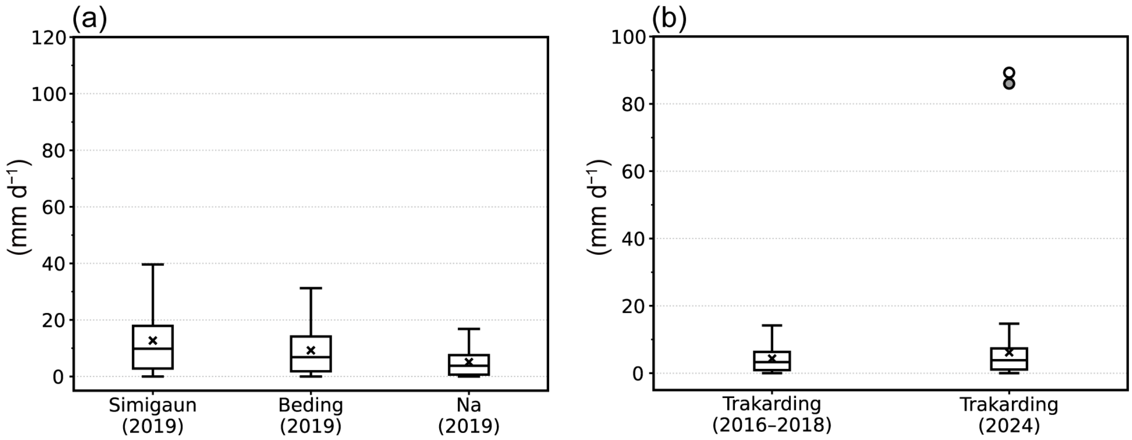

Fig. S7. (a) Boxplots of daily precipitation (mm d^{-1}) based on rain gauge data from the Simigaun, Beding, and Na stations in the Rolwaling region from 1 June to 30 September 2019 (Fujinami et al. 2022). (b) As in (a) but for Trakarding Glacier station based on June–September data from (left) 2016, 2017 and 2018 (Fujita et al. 2021) and (right) 2024. Gray and open circles above the boxplot in 2024 indicate daily precipitation rate for 27 and 28 September 2024, respectively

References:

Fujita K, Sunako S, Sakai A (2021) Meteorological observations at Trakarding Glacier Automatic Weather Station, Rolwaling, Nepal, 2016–2019. PANGAEA. https://doi.org/10.1594/PANGAEA.931159

Fujinami H, Fujita K, Sato Y, Kanamori H, Kayastha R, Kayastha RB (2022) Precipitation observations in Rolwaling Valley, eastern Nepal Himalayas, in summer 2019. PANGAEA. https://doi.org/10.1594/PANGAEA.943230

Kikuchi K (2021). The boreal summer intraseasonal oscillation (BSISO): A review. J Meteorol Soc Jpn 99:933–972. https://doi.org/10.2151/jmsj.2021-045